Charge density wave collapse of $NbSe_2$ in the $(LaSe)_{1.14}(NbSe_2)_2$ misfit layer compound

Ludovica Zullo [1,2,*,†], Grégory Setnikar [3,*], Amit Pawbake [3], Tristan Cren [2], Christophe Brun [2], Justine Cordiez [4], Shunsuke Sasaki [4], Laurent Cario [4], Giovanni Marini [1], Matteo Calandra [1,2] and Marie-Aude Méasson [3,‡]

[1]*Department of Physics, University of Trento, Via Sommarive 14, 38123 Povo, Italy*

[2]*Sorbonne Université, CNRS, Institut des Nanosciences de Paris, UMR7588, F-75252 Paris, France*

[3]*CNRS, Université Grenoble Alpes, Institut Néel, 38042 Grenoble, France*

[4]*Nantes Université, CNRS, Institut des Matériaux de Nantes Jean Rouxel, IMN, F-44000 Nantes, France*

(Received 24 May 2024; revised 25 July 2024; accepted 26 July 2024; published 28 August 2024)

Misfit layer compounds, heterostructures composed of a regular alternating stacking of rocksalt monochalcogenide bilayers and few-layer transition-metal dichalcogenides, are an emergent platform to investigate highly doped transition-metal dichalcogenides. Among them, $(LaSe)_{1.14}(NbSe_2)_2$ displays Ising superconductivity, while the presence of a charge density wave (CDW) in the material is still under debate. Here, by using polarized Raman spectroscopy and first-principles calculations, we show that $NbSe_2$ undergoes a doping-driven collapse of the CDW ordering within the misfit, and no signature of the CDW is detected down to 8 K. We provide a complete experimental and theoretical description of the lattice dynamics of this misfit compound. We show that the vibrational properties are obtained from those of the two subunits, namely, the LaSe unit and the $NbSe_2$ bilayer, in the presence of a suitable field-effect doping, and then highlight the two-dimensional nature of the lattice dynamics of $NbSe_2$ within the $(LaSe)_{1.14}(NbSe_2)_2$ three-dimensional structure.

DOI: 10.1103/PhysRevB.110.075430

I. INTRODUCTION

Transition-metal dichalcogenides (TMDs) are a wide family of layered materials possessing fascinating physical phenomena [1–4]. Among these, bulk $NbSe_2$ displays competition between the charge density wave (CDW) and superconducting order. An incommensurate CDW transition at 33 K occurs in bulk 2H-$NbSe_2$ [5–7]. Superconductivity (SC) emerges below 7.2 K and coexists with the CDW state [8]. Recent experiments [9,10] demonstrate that CDW survives in the two-dimensional (2D) limit for $NbSe_2$ bilayers and single layers.

Achieving complete control of the CDW order in these systems could lead to a better understanding of the interplay between SC and CDW. To this aim, external parameters that can be tuned are doping, pressure, strain, and sample thickness. However, each one of these control knobs leads to different effects. For example, applying pressure to bulk $NbSe_2$ leads to a suppression of the CDW at ≈4.4 GPa and an increase of the superconducting T_c [11], but no change in the ordering vector occurs. In the bulk, electron doping can be achieved via chemical intercalation [12], paving the way to a tunability of the ordering vector. Exfoliation of 2D TMDs and ionic-liquid-based field-effect transistors has led to the possibility of setting the doping electrochemically by tuning the voltage drop at the capacitor plates to generate an electrical double layer in the proximity of the 2D dichalcogenide [13]. Experiments show that the CDW phase in bilayer $NbSe_2$ is weakened by electron doping [14]. This suggests that it could be possible to observe a CDW collapse at high voltages. Unfortunately, the amount of doping required to observe a collapse of the CDW phase exceeds the largest carrier chargings that are accessible via field-effect gating ($n_e \approx 3 \times 10^{14}$ e$^-$ cm^{-2}). Other approaches are thus needed to achieve higher doping.

Misfit layer compounds (MLCs) are an intriguing alternative for achieving nearly perfectly integrated 2D TMDs with massive doping [15–18]. These heterostructures are formed by few-layer TMDs alternated with rocksalt units along the stacking direction. The rocksalt units are electron donors and act as ultraefficient parallel plate capacitors [18] with a substantially boosted voltage drop at the rocksalt/TMD interface, much larger than the one achievable via conventional or electrical double-layer field-effect transistors. This leads to a massive electron charge transfer from the rocksalt to the TMDs.

We focus here on the misfit layer compound $(LaSe)_{1.14}(NbSe_2)_2$ that is composed of two subsystems, namely, bilayers $NbSe_2$ (subsystem 1) and LaSe rocksalt subunits (subsystem 2) with different symmetries and periodicity [19]. The lattice parameter's mismatch along one of the in-plane directions of ratio $|\mathbf{a_2}|/|\mathbf{a_1}| = 6/3.437$ (≈ 7/4) makes $(LaSe)_{1.14}(NbSe_2)_2$ an incommensurate compound. Quasiparticle interference measurements (QPIs) and angle-resolved photoemission spectroscopy (ARPES) show that each monolayer of $NbSe_2$ inside the $(LaSe)_{1.14}(NbSe_2)_2$ MLC is strongly electron doped with a large Fermi level shift of +0.3 eV, (corresponding to $n_e \approx 6 \times 10^{14}$ e$^-$ cm^{-2}) [17]. Furthermore, scanning tunneling microscopy (STM) and magnetotransport measurements demonstrate that bulk $(LaSe)_{1.14}(NbSe_2)_2$ is superconducting at 5.7 K with a critical

*These authors contributed equally to this work.
†Contact author: ludovica.zullo@unitn.it
‡Contact author: marie-aude.measson@neel.cnrs.fr

field in the TMD plane that strongly violates the Pauli limit due to an efficient Ising protection, as in the monolayer case [20].

Although superconductivity in $(LaSe)_{1.14}(NbSe_2)_2$ has been clearly demonstrated, the occurrence of CDW is still under debate. STM topography detected the presence of a short-range 2×2 modulation disappearing above 105 K [17]. However, the 2×2 modulation observed in $(LaSe)_{1.14}(NbSe_2)_2$ by STM could be ascribed to a nonuniform doping on the cleaved surface. No bulk sensitive probes have demonstrated the presence or absence of a CDW in $(LaSe)_{1.14}(NbSe_2)_2$ up to now.

In this work, by performing Raman measurements and first-principles electronic structure calculations, we demonstrate a CDW collapse in the $NbSe_2$ bilayers of $(LaSe)_{1.14}(NbSe_2)_2$ and ascribe it to the large electron transfer from the rocksalt to the TMD layers. We assign the most intense Raman peaks to either of the MLC subunits (rocksalt or TMD) by comparing experimental Raman data and calculations. Finally, we show that as it happens for the electronic structure [18], the vibrational properties of MLC can be efficiently modeled by using a simple field-effect transistor scheme where each subunit can be seen as the gate of a parallel plate capacitor. Our work sets a reference scheme for the interpretation of vibrational and structural properties of misfit layer compounds that can be extended to other compounds of the same family.

The paper is structured as follows: in Sec. II, we describe the system and give the technical details of our experiment and first-principles calculations. In Sec. III, we examine the theoretical rationale for the CDW stability of $NbSe_2$ inside the misfit. In Sec. IV, we discuss the collapse of CDW ordering in $(LaSe)_{1.14}(NbSe_2)_2$. In Sec. V, we present the Raman response of $(LaSe)_{1.14}(NbSe_2)_2$ and discuss the mode attribution in comparison with the theory, and, finally, in Sec. VI, we draw our conclusions.

II. METHODS

A. Experiment

Two single crystals of $(LaSe)_{1.14}(NbSe_2)_2$ were prepared by vapor transport using I_2, as detailed in Ref. [17]. X-ray powder-diffraction experiments confirmed the so-called 1Q2H structure [17], namely, an alternated stacking of LaSe bilayers (NaCl structure) with TMD bilayers of $NbSe_2$ (polytype 2H), as shown in Fig. 1. Samples were freshly cleaved perpendicular to the [001] axis just before performing Raman experiments in vacuum. Polarized Raman scattering has been performed in quasibackscattering geometry with an incident laser line at 532 nm from a solid-state laser. The laser heating rate is evaluated at 1 K/mW. We used a closed-cycle ^{4}He cryostat for the measurements from 8 to 300 K. The scattered light was analyzed by a Jobin Yvon T64000 triple subtractive grating spectrometer equipped with a cooled CCD detector. By keeping the optical setup identical during the measurements, the Raman signal is quantitative. In particular, the comparison of the intensity of the spectra between different temperatures is meaningful and no normalization has been applied. The contribution of the Bose factor has been removed from all spectra, with the temperatures corrected from the laser heating.

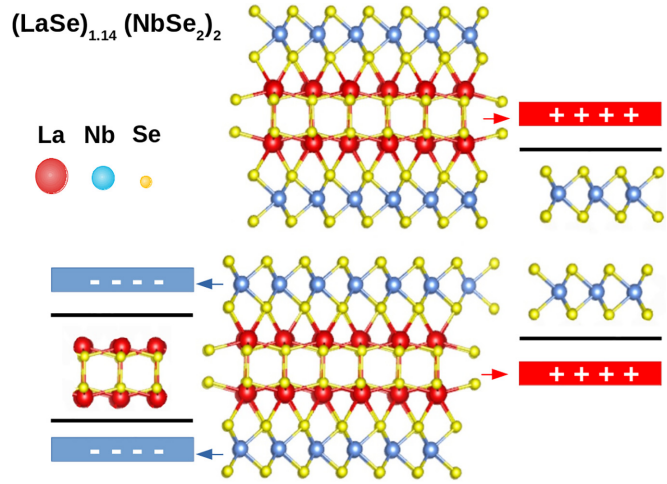

FIG. 1. Crystal structure of $(LaSe)_{1.14}(NbSe_2)_2$ (center) composed of LaSe bilayers (red and yellow) and $NbSe_2$ bilayers (blue and yellow). Each LaSe bilayer donates ≈0.6 electrons/Nb to each $NbSe_2$ layer. The $NbSe_2$ bilayer is modeled in a field-effect transistor setup (right), in which each LaSe bilayer is replaced by a charged plate having a positive charge of 0.6 electrons per Nb atom. The LaSe bilayer is modeled in a field-effect transistor setup, replacing each $NbSe_2$ bilayer by a negatively charged plate of 0.6 electrons per Nb. To confine the atoms in the region in between the charged plates, positive potential barriers are added (black lines).

B. Theory

1. Crystal structure

Given the incommensurability of the misfit layer compounds along one of the in-plane directions, a $(3 + 1)$D superspace group could be adopted to label the crystal structures [16]. However, the commensurate approximant of the $(LaSe)_1.14(NbSe_2)_2$ compound crystallizes in the $P1$ space group. The number of expected phonons is large, virtually infinite due to the incommensurability. From the symmetry analysis derived from the $P1$ symmetry, all modes are both Raman (R) and Infrared (IR) active. However, many of the potentially Raman active modes have very low intensity as (i) the symmetry of the subunits closely resembles the one of the isolated counterparts and (ii) the $P1$ group arises from the need to match the rocksalt and TMD space groups.

In order to gain a better understanding of the Raman active phonon modes, we first consider the two substructures as separated, namely, a rocksalt bilayer of LaSe and a bilayer of 2H-$NbSe_2$ (2L-$NbSe_2$). Along the c axis, one bilayer of $NbSe_2$ corresponds to one unit cell of 2H-$NbSe_2$.

In the presence of mirror symmetry with respect to the Nb plane (i.e., isolated $NbSe_2$ bilayer in the absence of an external electric field), the 2L-$NbSe_2$ substructure belongs to the space group $P\bar{3}m1$ (no. 164, D^3_{3d} point group). Each bilayer has six atoms per unit cell. The Wyckoff positions of the two Nb atoms are $2c$ (with $z = 3.13$ Å), while the four Se are in $2d$ (with $z = 1.47$ Å) and $2d$ (with $z = 4.84$ Å), respectively.

Bulk LaSe crystallizes in the $Fm\bar{3}m$ (no. 225) space group with two atoms per cell. However, we choose to label

the atomic positions of the isolated LaSe bilayer by using the *Cmm*2 space group (no. 35, C_{2v} point group), which is suitable for the orthorhombic lattice of LaSe within the misfit. The LaSe bilayer is an alternation of La and Se with a total of eight atoms per unit cell. The four atoms composing the first layer have Wyckoff positions 2*a* (with $z = -0.077$ Å) for Se and 2*b* (with $z = -0.076$ Å) for La. The four atoms composing the second layer have Wyckoff positions 2*a* (with $z = 0.076$ Å) for La and 2*b* (with $z = 0.077$ Å) for Se.

In our calculations, the in-plane lattice parameter of all the considered structures is fixed as the one of each subsystem in the bulk $(LaSe)_{1.14}(NbSe_2)_2$, namely, $a_1 = 3.437$ Å and $a_2 = 6$ Å [17].

2. Modeling of the bulk misfit

Bulk $(LaSe)_{1.14}(NbSe_2)_2$ is a periodic arrangement of LaSe and $NbSe_2$ subunits along the stacking direction. The lattice parameter mismatch in one of the in-plane directions makes the misfit cell incommensurate. It is possible to simulate an approximate commensurate cell [17] by considering the ratio $|\mathbf{a_2}|/|\mathbf{a_1}| = 6/3.437$ ($\approx 7/4$), and thus $m = 7|\mathbf{a_1}| \approx 4|\mathbf{a_2}|$. This periodic approximant has been used to calculate the electronic structure [17], however, it is still formed by too many atoms for the calculation of the vibrational properties. In order to reduce the computational effort, we approximate the 7/4 mismatch ratio by 8/4, corresponding to a 2/1 ratio. This is done by applying 14.6% tensile strain to the rocksalt subunit, increasing the lattice parameter to $a_2 = 6.875$ Å. The $NbSe_2$ in-plane parameter is, on the contrary, kept the same as in the misfit ($a_1 = 3.437$ Å).

Consequently, the two subunit cells in the 2×1 periodic approximant of bulk $(LaSe)_{1.14}(NbSe_2)_2$ are listed below. The $NbSe_2$ sublattice has an orthorhombic cell with in-plane lattice vectors $a_1 = 3.437$ Å and $b_1 = 6$ Å, while the LaSe sublattice has an orthorhombic cell with in-plane lattice vectors $a_2 = 6.875$ Å and $b_2 = 6$ Å.

The resulting misfit crystal has an orthorhombic cell with lattice parameters $a = |\mathbf{b_1}| = |\mathbf{b_2}| = 6$ Å, $b = 2|\mathbf{a_1}| \approx 1|\mathbf{a_2}| = 6.875$ Å, and $c = 18.25$ Å. The structure has a *P*1 symmetry and includes 32 atoms in the cell (atomic positions are reported in Table I of the Supplemental Material (SM) [21]).

We calculate the vibrational properties of bulk $(LaSe)_{1.14}(NbSe_2)_2$ by means of density functional perturbation theory (DFPT) as implemented in the QUANTUM ESPRESSO (QE) code [22,23]. We choose to employ the optimized ultrasoft pseudopotentials from pslibrary [24] to reduce the computational effort. The kinetic energy cutoff is set to 40 Ry and the Brillouin-zone (BZ) integration is carried out over a $4 \times 4 \times 2$ electron-momentum Monkhorst-Pack grid and by using a Gaussian smearing of 0.01 Ry. The Perdew-Burke-Ernzerhof (PBE) [25] exchange and correlation functional is used in the calculations.

The atomic positions are fully optimized by means of the Broyden-Fletcher-Goldfarb-Shannon (BFGS) algorithm, with a convergence threshold of 10^{-4} Ry on the total energy difference between consecutive structural optimization steps and of 10^{-3} Ry/Bohr on all forces components. During the relaxation procedure, we use the van der Waals corrections Grimme-D3 [26] to reproduce the interaction among adjacent $NbSe_2$ layers.

We compute the dynamical matrix of bulk $(LaSe)_{1.14}(NbSe_2)_2$ at the Γ point. The phonon density of states (PHDOS) is obtained by Fourier interpolation over a $10 \times 10 \times 1$ phonon-momentum grid and by using a Gaussian smearing of 3 cm^{-1}. We note that in our calculations, the shearing mode along the axis with the lattice mismatch among the $NbSe_2$ and LaSe units goes slightly imaginary; nevertheless, this is an artifact caused by the tensile strain applied to the LaSe subunit.

3. Modeling of the bulk misfit as a collection of field-effect transistors

Inside the misfit, the LaSe subunit acts as a donor, losing ≈1.2 electrons and donating ≈0.6 electrons per Nb atom to each monolayer of the $NbSe_2$ bilayer subunit [17]. By means of the field-effect transistor (FET) setup developed in Refs. [27,28], it is then possible to model the effect of the misfit structure onto the $NbSe_2$ bilayer by using a bilayer TMD sandwiched between two uniformly positive charged gates (see Fig. 1). Each charged gate replaces the rocksalt (RS) subunit and has a positive charge per Nb corresponding to 0.6 times the modulus of the electronic charge. This approach was efficiently carried out to estimate the misfit electronic structure in Ref. [18].

The field-effect scheme can also be employed by considering an RS subunit sandwiched between two uniformly negative-charged gates (see Fig. 1). In this case, the goal is to determine the effect of the misfit structure onto the LaSe bilayer subunit so that the charged plates are now negatively charged.

The field-effect modeling is carried out by using density functional theory (DFT) as implemented in the QUANTUM ESPRESSO (QE) [22] package using the PBE exchange and correlation functional [25]. We employ ultrasoft pseudopotentials from the Vanderbilt distribution for La and Nb, including semicore states for Nb atoms [29], while for Se, we use norm-conserving pseudopotentials with empty *d* states in the valence. The kinetic energy cutoff for the plane-wave basis set of $NbSe_2$ (LaSe) is set to 50 (48) Ry. The Brillouin-zone (BZ) integration is performed with a Monkhorst-Pack grid of $21 \times 21 \times 1$ ($14 \times 14 \times 1$) *k* points and a Gaussian smearing of 0.01 (0.015) Ry. The smearing value of 0.01 Ry is proven to ensure the convergence of the phonon frequencies of $NbSe_2$ within 1 cm^{-1}.

A Coulomb long-range interaction cutoff is placed at $z_{cut} = c/2$, with c the unit-cell size in the direction perpendicular to the plane: c is set opportunely for each of the different systems to 20 Å for LaSe and 25 Å for $NbSe_2$. Each of the two subsystems is centered around $z = 0$. For 2L-$NbSe_2$ (LaSe), we use a double-gate configuration, with two charged plates at $z_{bot} = -0.266c$ ($z_{bot} = -0.221c$) and $z_{top} = +0.266c$ ($z_{top} = +0.221c$), each with a charge of ρ=+0.6 ($\rho = -0.6$) times the modulus of the electronic charge, such that $\rho_{tot} = \rho_{2L} + \rho_{bot} + \rho_{top} = 0$. For each system, a potential barrier V of height 2.5 Ry is placed before the gates at $z_V = z_{bot} + 0.1$ ($z_V = z_{top} - 0.1$) in order to confine the atoms between the gate electrodes.

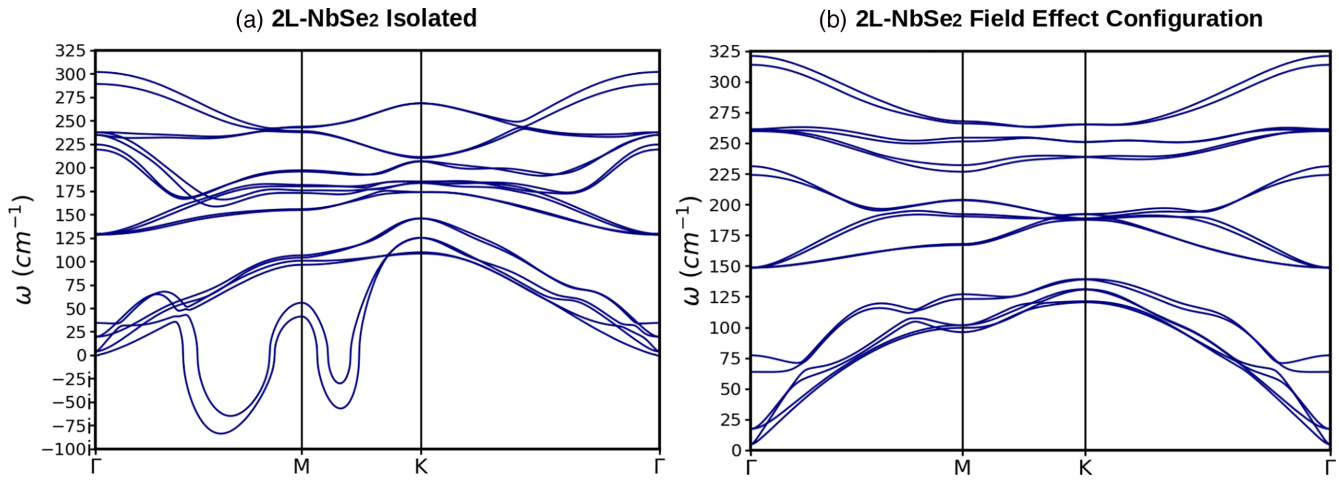

FIG. 2. Calculated phonon dispersion along the Γ-*M*-*K*-Γ path of (a) an isolated 2L-$NbSe_2$ and (b) a field-effect doped 2L-$NbSe_2$. In (b), the charge density wave instability is clearly removed by electron doping.

The Raman active phonon frequencies are calculated using density functional perturbation theory (DFPT) in the linear response regime [23]. In order to fulfill the 7/4 lattice mismatch ratio of the best periodic approximant, the dynamical matrices are calculated on uniform $7 \times 7 \times 1$ and $4 \times 4 \times 1$ phonon-momentum grids and then Fourier interpolated in the full Brillouin zone. For the DOS at zone center in Fig. 4(b), we use only the phonon frequencies obtained from the dynamical matrices on a $4 \times 1 \times 1$ phonon-momentum grid.

The individual phonon densities of states (PHDOS) in Fig. 5 are obtained by Fourier interpolation over a $40 \times 40 \times 1$ and $70 \times 70 \times 1$ phonon-momentum grid for LaSe and $NbSe_2$, respectively, and by using a Gaussian smearing of 3 cm^{-1}.

Vibrational properties of isolated neutral 2L-$NbSe_2$ are calculated using DFPT in the linear response regime on uniform $8 \times 8 \times 1$ phonon-momentum grids. The Brillouin-zone integration is performed with a Monkhorst-Pack grid of $30 \times 30 \times 1$ k points and a Methfessel-Paxton smearing of 0.005 Ry.

III. CDW STABILITY IN THE MISFIT STRUCTURE

In Fig. 2, we calculate the harmonic phonon dispersion of an isolated neutral $NbSe_2$ bilayer [Fig. 2(a)] and of a $NbSe_2$ bilayer in a field-effect configuration with a charging corresponding to 0.6 electrons per niobium atom [Fig. 2(b)]. The charge density wave instability occurring in the isolated $NbSe_2$ bilayer is showcased by the presence of an imaginary phonon band with the most imaginary value at $\mathbf{q} \approx 2/3\mathbf{\Gamma M}$. Anharmonic effects do not qualitatively alter this since the instability is reduced, but its wave vector is preserved [30]. In the FET-charged $NbSe_2$ bilayer [Fig. 2(b)], the CDW instability is completely removed for charge transfers similar to those in the misfit. We thus expect that the CDW should collapse once the $NbSe_2$ subunit is inserted in the misfit. We will see that this prediction is confirmed by Raman data.

We believe that our FET simulation can accurately recreate CDW behavior as a function of misfit doping level. Indeed, in the first place, it has been demonstrated that the misfit generally behaves as a periodic arrangement of tunable field-effect transistors [18]. In addition, in the specific case of $(LaSe)_{1.14}(NbSe_2)_2$, the electronic band structure of the misfit can be assimilated as that of a rigidly doped $NbSe_2$ single layer [17]. Second, because the CDW in $NbSe_2$ originates from the in-plane modes, FET modeling is appropriate for characterizing its physics. Our FET approach is able to correctly capture the charge-transfer-induced CDW melting in good agreement with the experimental results, despite missing the possible electron-phonon coupling modifications due to the interface, whose inclusion would require linear response calculations on a large supercell of 232 atoms.

Finally, we conclude by noting that if the charged plates mimicking the charge transfer by the LaSe subunits are removed and the FET charging is replaced by a uniform background doping, the results are completely different as they show an instability at the M point, in qualitative disagreement with experiments (see, for example, the supplemental materials of Ref. [17]). The reason is that in the misfit, as in a field-effect transistor, the charge transfer to the $NbSe_2$ bilayer is not uniformly distributed along the c axis. For this reason, the uniform background doping approximation is inappropriate.

IV. CHARGE-TRANSFER-DRIVEN CHARGE DENSITY WAVE COLLAPSE

Raman spectroscopy offers a direct probe of charge density wave signatures in the bulk [31,32] and in few-layer systems [9]. Two types of new Raman active modes arise as a fingerprint of the CDW. The first one is a soft phonon called the amplitude mode, that gradually hardens when cooling down and that arises from the phonon branch which softens at the CDW wave vector. This mode has been detected in bulk 2H-$NbSe_2$ at $\approx$40 cm^{-1} [triangle in Fig. 3(c)] [33,34]. The second type of new peaks are zone-folded modes that arise from other phonon bands at the CDW wave vector. These modes are folded into Γ by the effect of the CDW modulation and are therefore detectable [stars in Fig. 3(c)].

Figures 3(a) and 3(b) show the Raman response of $(LaSe)_{1.14}(NbSe_2)_2$ in crossed and parallel polarizations for temperatures ranging from 8 to 200 K. In both polarizations,

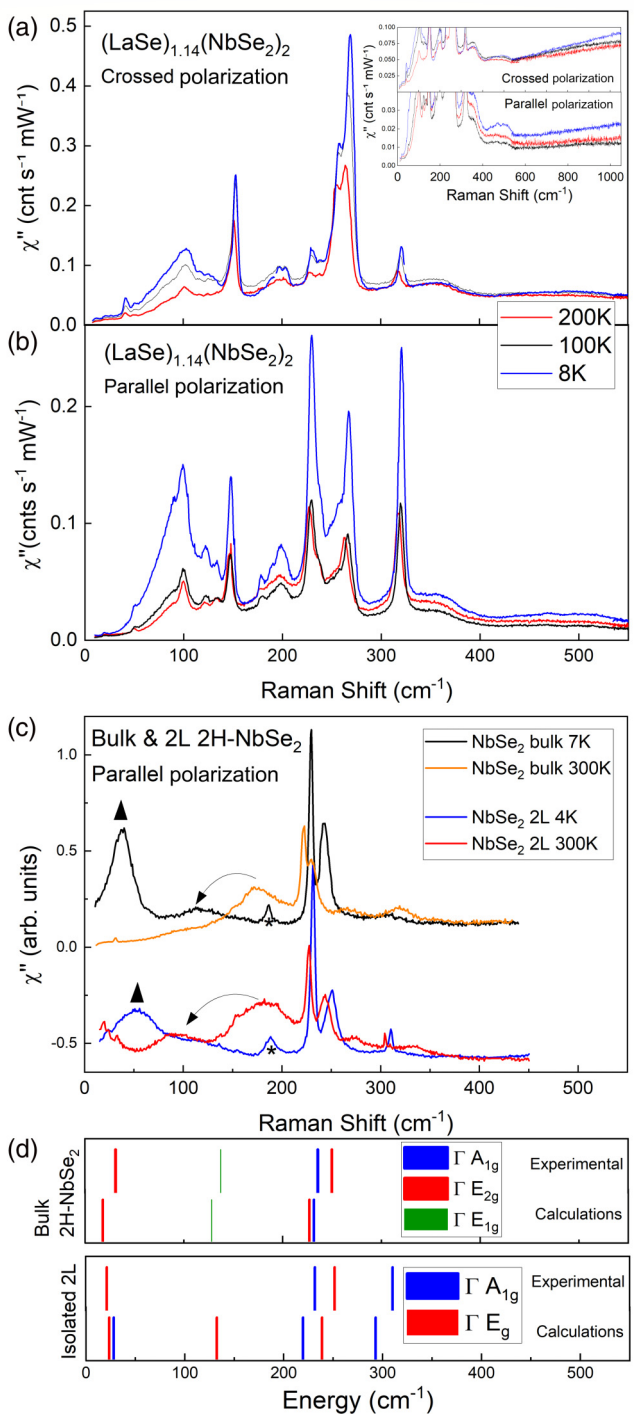

FIG. 3. Temperature dependence of the Raman response of $(LaSe)_{1.14}(NbSe_2)_2$ with the (*ab*)-plane (a) crossed and (b) parallel polarization configurations. Inset: Large energy-range electronic Raman response. (c) Raman response of bulk 2H-$NbSe_2$ and isolated 2L-$NbSe_2$ [37] at 300 and ∼5 K, in the CDW state. The stars and triangles stands for the Brillouin-zone folded phonons and amplitudons, respectively. The arrows indicate the double phonon modes related to the soft phonon branches of the CDW. (d) Raman active phonons energies from experiments and from theory.

a substantial increase of the overall intensity is measured when cooling down. Narrow phonon modes are reported up to 350 cm^{-1}. The modes above 350 cm^{-1} are broader and are most likely due to double phonon excitations.

Globally, the phonon modes harden when cooling down, as generally expected from anharmonic effect. No new modes appear at low temperatures, either across the temperature range where STM detected small patches with short range 2×2 modulation (100 K) [17] or across the temperature range at which the CDW is detected in bulk samples (35 K). The large-range electronic response does not present any signature of electronic gap opening that is sometimes measured in the CDW state [35,36].

The last possible fingerprint of the presence of a CDW is a two-phonon Raman feature from the soft phonon branch at $\mathbf{Q}_{CDW}$, i.e., the phonon momentum related to the CDW instability. In bulk 2H-$NbSe_2$, it is visible in Fig. 3(c), as indicated by the arrow. The only candidate for this experimental Raman feature is the broad mode in the low-energy range around 100 cm^{-1}, which is detected in both polarization configurations. However, the temperature dependence of this mode is peculiar and in stark contradiction with the behavior of the double phonon mode in $NbSe_2$. Indeed, as shown in Fig. 3(c), in bulk 2H-$NbSe_2$ the double phonon feature loses intensity in both the A_{1g} and E_{2g} symmetries and softens with decreasing temperature. Conversely, in the case of our $(LaSe)_{1.14}(NbSe_2)_2$, the large spectral weight bump always remains in the same energy range, and its intensity largely grows when cooling down, as shown in Fig. 3. So even if this part of the spectra could be partially due to two-phonon scattering, it does not evidence a softening of the branch and, thus, it is not related to a CDW. A comparison with DFT calculations suggests that the nature of the broad mode in the misfit can be attributed to the presence of a dense population of LaSe modes that overlap with a few low-energy $NbSe_2$ frequencies. Overall, these measurements suggest that no amplitude modes or CDW related modes occur down to 8 K.

We comment here on the CDW signatures observed by STM at the cleaved $(LaSe)_{1.14}(NbSe_2)_2$ surface, while no signature in the bulk could be detected by Raman spectroscopy. Investigation of the Raman response of 2H-$NbSe_2$ as a function of quality of the samples, as stated by the residual resistivity ratio (RRR = 50 for good samples and = 6 for the worst samples), clearly shows that the main CDW signature observed by Raman spectroscopy, namely, the amplitudon, has extremely weak intensity in low-quality samples [38]. A first hypothesis would be that the CDW would exist in the bulk, but with a very short coherence length of ≈2 nm, as suggested by the STM experiment. In this case, the situation would be somehow analogous to the one observed in the normal state of 2H-$NbSe_2$, where it is reported that short-range CDW modulations are observed by STM near the defects much above the bulk CDW critical temperature [39–41], while no Raman signatures are detected in this temperature regime. A second hypothesis would be that a surface peculiar behavior would stabilize and enhance a surface CDW, while its bulk counterpart would develop at much lower temperature and with lower amplitude and coherence length, or even not form at all. There have been reports of such complicated and different surface versus bulk CDW properties in well-known quasi-one-dimensional materials such as $NbSe_3$ or the blue bronze [42–44].

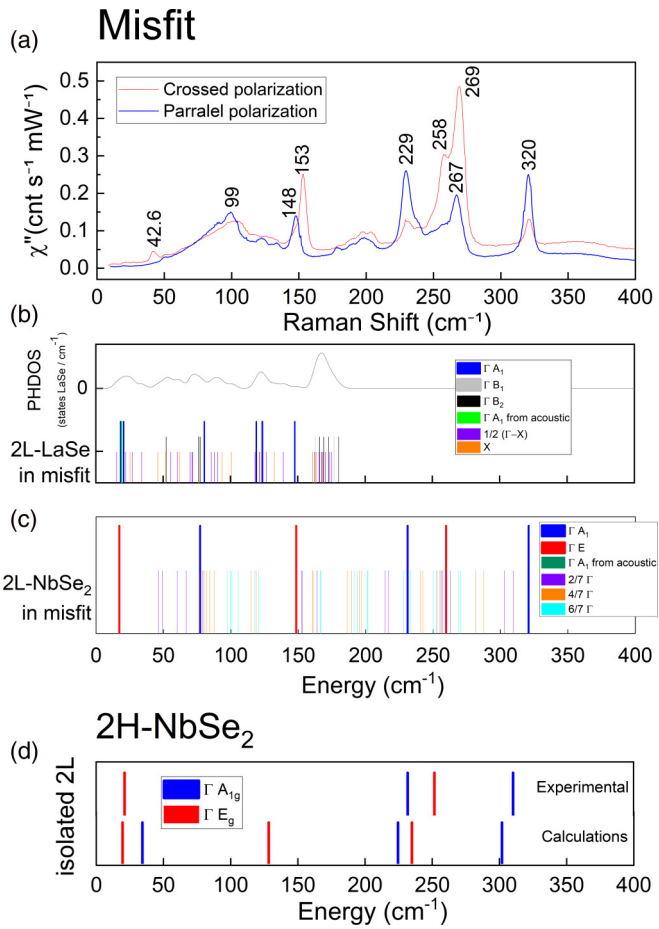

FIG. 4. (a) Raman spectra of $(LaSe)_{1.14}(NbSe_2)_2$ at 8 K in crossed and parallel polarizations in the (*ab*) plane. (b),(c) Theoretical calculations of Raman active modes of $(LaSe)_{1.14}(NbSe_2)_2$ obtained from those of the two subsystems, namely, (b) LaSe and (c) $NbSe_2$, electron doped by means of the FET setup. The original modes from Γ of the 1×1 cell (long bars) and their subsequent BZ folding (short bars) modes are indicated (see text). Original modes from Γ of the 1×1 cell are classified by symmetries. The phonon density of states of LaSe is shown in the upper part of (b). (d) Comparison between experimental [37] and theoretical zone center modes of isolated 2L-$NbSe_2$. Here, the $NbSe_2$ lattice parameter is the one in the misfit, namely, $a = 3.437$ Å.

V. RAMAN SCATTERING AND MODE ATTRIBUTION

In Fig. 4, we show the Raman spectra of $(LaSe)_{1.14}(NbSe_2)_2$ at 8 K in both parallel and crossed polarizations. There is a substantial difference among the two spectra, supporting a strong dependence of the signal on the symmetry of the modes. In Table I, we report the most intense modes together with their Raman active channels.

By comparing with the experimental Raman spectra in the bulk and in the 2L-$NbSe_2$ in Figs. 3(c) and 3(d), we notice a striking resemblance on the symmetry of the most intense modes, especially at high energy. Notably, in the 2L system, in addition to the expected three modes of the bulk 2H-$NbSe_2$, namely, one $E_{(2)g}$ interlayer mode at ∼30 cm^{-1}, and one A_{1g} and one $E_{(2)g}$ mode at ∼250 cm^{-1}, Lin *et al.* [37] report one additional mode due to the few-layer structures, namely, an A_{1g} mode at high-energy 310 cm^{-1}. A mode at ∼155 cm^{-1} is possibly measured by Lin *et al.*, but would require some confirmation. Importantly, these modes, even if measured at low temperature, are not due to the CDW ordering. As shown in Fig. 3(d), the energy and symmetry of the modes are well reproduced by our calculations for both systems, with a general tendency to underestimate their energy compared to the experimental results. As a straightforward interpretation of the spectra, we then tentatively assigned the most intense modes in the misfit to the modes of the same symmetry in the two-layer structure. As shown in Table I, there is a good correspondence with four modes, in terms of energy and symmetry.

In order to further corroborate our analysis and perform a full assignment of the modes, we consider here the two subunits of the compounds, namely, LaSe and $NbSe_2$, as well as their interplay. As the space group of the bulk misfit compound is P_1, all vibrational modes are Raman active. Thus, in the absence of a charge density wave instability, besides the zone center modes related to the LaSe and $NbSe_2$ subunit cells, one expects (i) $NbSe_2$ modes at in-plane phonon momenta that are not at zone center in the $NbSe_2$ bilayer Brillouin zone, but are backfolded at the zone center in the misfit Brillouin zone due to the 7×1 $NbSe_2$ periodicity occurring in $(LaSe)_{1.14}(NbSe_2)_2$; (ii) LaSe modes at in-plane phonon momenta that are not at the zone center in the LaSe bilayer Brillouin zone, but are backfolded at the zone center in the misfit Brillouin zone due to the the 4×1 LaSe periodicity occurring in $(LaSe)_{1.14}(NbSe_2)_2$; (iii) modes arising from the presence of two inequivalent $(LaSe)_{1.14}(NbSe_2)_2$ units along the *c* axis of the misfit unit cell (see Fig. 1); and, finally, (iv) modes that cannot be interpreted as pure LaSe or $NbSe_2$ modes.

As we will see later from PHDOS calculations of the whole misfit, practically all modes can be interpreted as modes of the two separated subunits. Thus, the occurrence of phonon modes that are mixed modes of the LaSe and $NbSe_2$ subunits can be excluded, and point (iv) can be neglected. The splitting of phonon frequencies due to the presence of two inequivalent $(LaSe)_{1.14}(NbSe_2)_2$ units along the *c* axis, i.e., point (iii), is also expected to be negligible as the $(LaSe)_{1.14}(NbSe_2)_2$ units are weakly interacting along the *c* axis. It then follows that an attempt to interpret the Raman response in terms of the backfolded modes of the $NbSe_2$ and LaSe subunits should lead to a clear understanding of the Raman spectra. Thus, we proceed to a more detailed analysis based on the Raman activity of the isolated and charged LaSe and $NbSe_2$ bilayers.

The LaSe rocksalt subunit (no. 35, C_{2v} point group) has 24 Γ-point frequencies,

$$\Gamma_{\mathrm{LaSe}} = 8A_1 + 8B_1 + 8B_2.$$

From symmetry, we expect the B_1 and B_2 modes to be Raman active since there is no inversion center. Even so, the B_1 and B_2 modes are not expected to be measured in the configuration of measurement (with the Poynting vector along the *c* axis). On the contrary, the 8 A_1 modes are Raman active and mainly in the parallel configuration since they have a $(a-b)^2$ response in crossed polarization, leading to small intensities. To summarize, the only modes that can be identified in

TABLE I. Intense Raman active modes measured in $(LaSe)_{1.14}(NbSe_2)_2$ at 8 K with polarizations in the (*ab*) plane. The labels ⊥ and ∥ stand for crossed and parallel polarizations, respectively. The third column reports the experimental data in an isolated 2L-$NbSe_2$ [37]. Calculated phonon modes in the misfit structure originating from the Γ point of the unfolded Brillouin zone and from subunits of $NbSe_2$ and LaSe are given in the fourth and sixth columns, respectively. In the fifth column, the splitted E_g modes of the 8/4 misfit cell are given, which correspond to the former E_g of the $NbSe_2$ subunit (italicized numbers). The label X marks the single intense mode that we could not assign from the two subunits (see text).

Intense modes of $(LaSe)_{1.14}(NbSe_2)_2$ (cm^{-1})	Raman activity ⊥ or ∥	Experimental modes in 2L $NbSe_2$ (cm^{-1})	Calculated modes energy/symmetry from 2L-$NbSe_2$ at Γ (cm^{-1})	Calculated modes from splitted E_g in misfit (cm^{-1})	Calculated modes energy/symmetry from LaSe at Γ (cm^{-1})
42.6	⊥	$21/E_g$	$17.3/E_g$		
99.0	∥		$77.2/A_{1g}$		or $120.1/A_1$
148	∥				$148.9/A_1$
153	⊥	154 [a]	$148.5/E_g$		
229	∥	$232/A_{1g}$	$231.2/A_{1g}$		
258	⊥	$251.5/E_g$	*$259.7/E_g$*	*$251.5/E_g$*	
267	∥		X		X
269	⊥			*$258.7/E_g$*	
320	∥	$310.5/A_{1g}$	$320.9/A_{1g}$		

[a]X. Xi (private communication): This mode at 154 cm^{-1} may require experimental confirmation.

parallel polarization, expected from the pure rocksalt subsystem, have A_1 symmetry.

For the $NbSe_2$ bilayer having $P\bar{3}m1$ space group (no. 164, D^3_{3d} point group), the behavior of the modes is the following. We have 18 Γ-point frequencies as

$$\Gamma_{NbSe_2} = 3A_{1g} + 3E_g + 3A_{2u} + 3E_u.$$

The three completely symmetric A_{1g} modes are all Raman active only in parallel polarization. The three doubly degenerate E_g modes can be detected in both crossed and parallel polarizations. Finally, the A_{2u} and E_u are not Raman active. The symmetry of the Γ modes, as well as their activity in different polarization configurations, are reported in Table I, in the fourth and sixth columns.

In the table, we assign the calculated Γ frequencies to the most intense mode in the Raman spectra. As it can be seen, only one of the most intense modes can be ascribed to LaSe. A second one at 99 cm^{-1} could be either assigned to LaSe or $NbSe_2$ since both subunits present a parallel-active mode in this range of energy. The other peaks are all derived from the 2L-$NbSe_2$ subsystem. The physics of the Raman spectra at 8 K reveals that the lattice dynamics of $(LaSe)_{1.14}(NbSe_2)_2$ can be described in terms of that of its individual constituents.

To strengthen this statement, we can look at the PHDOS calculation on the $8/4 = 2/1$ periodic approximant of the full misfit, shown in Fig. 5. The results are compared in Fig. 5 with the phonon density of states of the two separated subunits as well as with their sum in the presence of a field-effect charging mimicking the charge transfer among the LaSe and $NbSe_2$ subunits. As depicted in Fig. 5, almost all features in the misfit PHDOS are fairly well explained in terms of the sum of the PHDOS of the two (field-effect charged) separated subunits. The only feature present in the misfit PHDOS, but not in the PHDOS of the two subunits, is a peak at ≈150 cm^{-1}. This peak is at slightly higher energies ≈165–170 cm^{-1} in the LaSe subunit. The difference is due to the strain applied to the LaSe subunit inside the misfit to obtain the 2/1 periodic approximant (14% strain), while the field-effect transistor (FET) charged LaSe bilayer is unstrained and has the same lattice parameters as in the bulk misfit. Overall, we can state that the vibrational properties of the $(LaSe)_{1.14}(NbSe_2)_2$ are entirely determined by those of the two separated subunits with an appropriate amount of charging.

From Fig. 5, it is also clear that due to the heavy La mass, the phonon modes of the RS subunit are mostly concentrated in the low-energy part of the spectrum (below 175 cm^{-1}), while those of the $NbSe_2$ bilayer occur at all energies.

As summarized in Table I, only two of the most intense Raman peaks, namely, the one at 269 cm^{-1} in crossed polarization and 267 cm^{-1} in parallel polarization, are not directly deducible from the modes of 2L-$NbSe_2$. We are able to assign the highly intense mode at 269 cm^{-1} in crossed polarization to the former double-degenerate high-energy E_g mode of 2L-$NbSe_2$ at 259 cm^{-1} that splits in the misfit.

In order to perform this assignment, we consider the full misfit calculation employing the $8/4 = 2/1$ periodic approximant (5), where the two distinct peaks can be clearly identified in this energy range. In order to check if these peaks originate

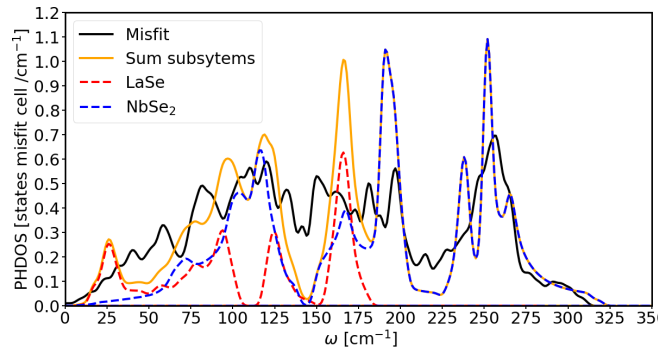

FIG. 5. Phonon density of states (PHDOS) per misfit formula unit of bulk $(LaSe)_{1.14}(NbSe_2)_2$ (black solid line). Comparison with the PHDOS of the individual subsystems: LaSe subunit doped of 1.2 electrons per unit cell in the FET setup (red dashed line), $NbSe_2$ bilayer doped of 0.6 electrons per Nb atom in the FET setup (blue dashed line), respectively, and with their sum (orange solid line).

from the E_g mode of the isolated FET-doped 2L-$NbSe_2$, we project all the full misfit phonon eigenvectors onto the ones corresponding to the doubly degenerate E_g mode at 259 cm^{-1} in the isolated FET-doped 2L-$NbSe_2$. We find that the highest E_g character is present in two modes at 251.5 and 258.7 cm^{-1} (see Table I, fifth column).

Note that we also evaluated the effect of the slight non-hexagonality of 2L-$NbSe_2$ within the misfit [17], which is just a very small, $\sim$1 cm^{-1}, splitting that cannot account for our experimental results (see the SM [21]).

Finally, only the intense mode at 267 cm^{-1} in parallel polarization is not captured by our DFT calculations. This one is most probably a hybrid mode of the system as a whole, caused by the bonding between the TMD and the RS subunits that we neglected in our calculations.

VI. CONCLUSIONS

By using polarized Raman spectroscopy and first-principles calculations, we provide a complete description of the vibrational properties of the misfit layer compound $(LaSe)_{1.14}(NbSe_2)_2$. We identify all the main phonon modes and their symmetry and demonstrate that similarly to what happens for the electronic properties, the vibrational properties can be understood in terms of the two subunits (LaSe and $NbSe_2$ bilayers) in a field-effect configuration, where the charging of the gates is directly determined by the charge transfer in the misfit structure. Notably, the lattice dynamics of the TMD has a strong 2D character in this 3D misfit structure. Finally, our theoretical understanding is supported by the Raman results, particularly by the charge density wave collapse in the misfit due to the large charge transfer from the LaSe subunit. Our work is relevant beyond the case of $(LaSe)_{1.14}(NbSe_2)_2$ as it sets a road map for the investigation of the large class of materials composed of misfit layer compounds.

ACKNOWLEDGMENTS

We thank Xiaoxiang Xi for fruitful exchanges of information. We thank Alex W. Chin for fruitful discussions. M.-A.M. thanks the European Research Council (ERC) under the European Union's Horizon 2020 research and innovation programme (Grant Agreement No. 865826). This work has received funding from the Agence Nationale de la Recherche under the project Misfit (Project No. ANR-21-CE30-0054). M.C. acknowledges support from ICSC – Centro Nazionale di Ricerca in HPC, Big Data and Quantum Computing, funded by the European Union under NextGenerationEU.

The views and opinions expressed here are those of the author(s) only and do not necessarily reflect those of the European Union or The European Research Executive Agency. Neither the European Union nor the granting authority can be held responsible for them.

[1] S. Manzeli, D. Ovchinnikov, D. Pasquier, O. V. Yazyev, and A. Kis, 2D transition metal dichalcogenides, Nat. Rev. Mater. **2**, 17033 (2017).

[2] Q. Fu, J. Han, X. Wang, P. Xu, T. Yao, J. Zhong, W. Zhong, S. Liu, T. Gao, Z. Zhang, L. Xu, and B. Song, 2D transition metal dichalcogenides: design, modulation, and challenges in electrocatalysis, Adv. Mater. **33**, 1907818 (2021).

[3] H. Chen, J. Zhang, D. Kan, J. He, M. Song, J. Pang, S. Wei, and K. Chen, The recent progress of two-dimensional transition metal dichalcogenides and their phase transition, Crystals **12**, 1381 (2022).

[4] S. Joseph, J. Mohan, S. Lakshmy, S. Thomas, B. Chakraborty, S. Thomas, and N. Kalarikkal, A review of the synthesis, properties, and applications of 2D transition metal dichalcogenides and their heterostructures, Mater. Chem. Phys. **297**, 127332 (2023).

[5] J. Wilson, F. Di Salvo, and S. Mahajan, Charge-density waves and superlattices in the metallic layered transition metal dichalcogenides, Adv. Phys. **24**, 117 (1975).

[6] D. E. Moncton, J. D. Axe, and F. J. DiSalvo, Neutron scattering study of the charge-density wave transitions in 2H-$TaSe_2$ and 2H-$NbSe_2$, Phys. Rev. B **16**, 801 (1977).

[7] C. D. Malliakas and M. G. Kanatzidis, Nb–Nb interactions define the charge density wave structure of 2H-$NbSe_2$, J. Am. Chem. Soc. **135**, 1719 (2013).

[8] E. Revolinsky, G. Spiering, and D. Beerntsen, Superconductivity in the niobium-selenium system, J. Phys. Chem. Solids **26**, 1029 (1965).

[9] X. Xi, L. Zhao, Z. Wang, H. Berger, L. Forró, J. Shan, and K. F. Mak, Strongly enhanced charge-density-wave order in monolayer $NbSe_2$, Nat. Nanotechnol. **10**, 765 (2015).

[10] M. M. Ugeda, A. J. Bradley, Y. Zhang, S. Onishi, Y. Chen, W. Ruan, C. Ojeda-Aristizabal, H. Ryu, M. T. Edmonds, H.-Z. Tsai, A. Riss, S.-K. Mo, D. Lee, A. Zettl, Z. Hussain, Z.-X. Shen, and M. F. Crommie, Characterization of collective ground states in single-layer $NbSe_2$, Nat. Phys. **12**, 92 (2016).

[11] O. Moulding, I. Osmond, F. Flicker, T. Muramatsu, and S. Friedemann, Absence of superconducting dome at the charge-density-wave quantum phase transition in 2H-$NbSe_2$, Phys. Rev. Res. **2**, 043392 (2020).

[12] Z. Wang, R. Li, C. Su, and K. P. Loh, Intercalated phases of transition metal dichalcogenides, SmartMat **1**, e1013 (2020).

[13] K. S. Novoselov, D. Jiang, F. Schedin, T. J. Booth, V. V. Khotkevich, S. V. Morozov, and A. K. Geim, Two-dimensional atomic crystals, Proc. Natl. Acad. Sci. **102**, 10451 (2005).

[14] X. Xi, H. Berger, L. Forró, J. Shan, and K. F. Mak, Gate tuning of electronic phase transitions in two-dimensional $NbSe_2$, Phys. Rev. Lett. **117**, 106801 (2016).

[15] J. Rouxel, A. Meerschaut, and G. Wiegers, Chalcogenide misfit layer compounds, J. Alloys Compd. **229**, 144 (1995).

[16] G. Wiegers, Misfit layer compounds: structures and physical properties, Prog. Solid State Chem. **24**, 1 (1996).

[17] R. T. Leriche, A. Palacio-Morales, M. Campetella, C. Tresca, S. Sasaki, C. Brun, F. Debontridder, P. David, I. Arfaoui, O. Šofranko, T. Samuely, G. Kremer, C. Monney, T. Jaouen, L. Cario, M. Calandra, and T. Cren, Misfit layer compounds: a

platform for heavily doped 2D transition metal dichalcogenides, Adv. Funct. Mater. **31**, 2007706 (2021).

[18] L. Zullo, G. Marini, T. Cren, and M. Calandra, Misfit layer compounds as ultratunable field effect transistors: from charge transfer control to emergent superconductivity, Nano Lett. **23**, 6658 (2023).

[19] R. Roesky, A. Meerschaut, J. Rouxel, and J. Chen, Structure and electronic transport properties of the misfit layer compound $(LaSe)_{1.14}(NbSe_2)_2$, $LaNb_2Se_5$, Z. Anorgan. Allgem. Chem. **619**, 117 (1993).

[20] P. Samuely, P. Szabó, J. Kačmarčík, A. Meerschaut, L. Cario, A. G. M. Jansen, T. Cren, M. Kuzmiak, O. Šofranko, and T. Samuely, Extreme in-plane upper critical magnetic fields of heavily doped quasi-two-dimensional transition metal dichalcogenides, Phys. Rev. B **104**, 224507 (2021).

[21] See Supplemental Material at http://link.aps.org/supplemental/10.1103/PhysRevB.110.075430 for additional data.

[22] P. Giannozzi, O. Baseggio, P. Bonfà, D. Brunato, R. Car, I. Carnimeo, C. Cavazzoni, S. De Gironcoli, P. Delugas, F. Ferrari Ruffino, A. Ferretti, N. Marzari, I. Timrov, A. Urru, and S. Baroni, QUANTUM ESPRESSO toward the exascale, J. Chem. Phys. **152**, 154105 (2020).

[23] S. Baroni, S. de Gironcoli, A. Dal Corso, and P. Giannozzi, Phonons and related crystal properties from density-functional perturbation theory, Rev. Mod. Phys. **73**, 515 (2001).

[24] A. D. Corso, Pseudopotentials periodic table: From H to Pu, Comput. Mater. Sci. **95**, 337 (2014).

[25] J. P. Perdew, K. Burke, and M. Ernzerhof, Generalized gradient approximation made simple, Phys. Rev. Lett. **77**, 3865 (1996).

[26] S. Grimme, S. Ehrlich, and L. Goerigk, Effect of the damping function in dispersion corrected density functional theory, J. Comput. Chem. **32**, 1456 (2011).

[27] T. Sohier, M. Calandra, and F. Mauri, Density functional perturbation theory for gated two-dimensional heterostructures: Theoretical developments and application to flexural phonons in graphene, Phys. Rev. B **96**, 075448 (2017).

[28] T. Brumme, M. Calandra, and F. Mauri, First-principles theory of field-effect doping in transition-metal dichalcogenides: Structural properties, electronic structure, Hall coefficient, and electrical conductivity, Phys. Rev. B **91**, 155436 (2015).

[29] D. Vanderbilt, Soft self-consistent pseudopotentials in a generalized eigenvalue formalism, Phys. Rev. B **41**, 7892 (1990).

[30] R. Bianco, L. Monacelli, M. Calandra, F. Mauri, and I. Errea, Weak dimensionality dependence and dominant role of ionic fluctuations in the charge-density-wave transition of $NbSe_2$, Phys. Rev. Lett. **125**, 106101 (2020).

[31] S. Sugai, K. Murase, S. Uchida, and S. Tanaka, Comparison of the soft modes in tantalum dichalcogenides, Physica B+C **105**, 405 (1981).

[32] J. C. Tsang, J. E. Smith, and M. W. Shafer, Raman spectroscopy of soft modes at the charge-density-wave phase transition in 2 H - $NbSe_2$, Phys. Rev. Lett. **37**, 1407 (1976).

[33] M.-A. Méasson, Y. Gallais, M. Cazayous, B. Clair, P. Rodière, L. Cario, and A. Sacuto, Amplitude Higgs mode in the 2H-$NbSe_2$ superconductor, Phys. Rev. B **89**, 060503(R) (2014).

[34] R. Grasset, T. Cea, Y. Gallais, M. Cazayous, A. Sacuto, L. Cario, L. Benfatto, and M.-A. Méasson, Higgs-mode radiance and charge-density-wave order in 2H-$NbSe_2$, Phys. Rev. B **97**, 094502 (2018).

[35] R. Grasset, Y. Gallais, A. Sacuto, M. Cazayous, S. Mañas-Valero, E. Coronado, and M.-A. Méasson, Pressure-induced collapse of the charge density wave and Higgs mode visibility in 2H-TaS_2, Phys. Rev. Lett. **122**, 127001 (2019).

[36] G. He, L. Peis, E. F. Cuddy, Z. Zhao, D. Li, Y. Zhang, R. Stumberger, B. Moritz, H. Yang, H. Gao, T. P. Devereaux, and R. Hackl, Anharmonic strong-coupling effects at the origin of the charge density wave in CsV_3Sb_5, Nat. Commun. **15**, 1895 (2024).

[37] D. Lin, S. Li, J. Wen, H. Berger, L. Forró, H. Zhou, S. Jia, T. Taniguchi, K. Watanabe, X. Xi, and M. S. Bahramy, Patterns and driving forces of dimensionality-dependent charge density waves in 2H-type transition metal dichalcogenides, Nat. Commun. **11**, 2406 (2020).

[38] R. Sooryakumar, M. V. Klein, and R. F. Frindt, Effect of nonmagnetic impurities on the Raman spectra of the superconductor niobium diselenide, Phys. Rev. B **23**, 3222 (1981).

[39] C. J. Arguello, S. P. Chockalingam, E. P. Rosenthal, L. Zhao, C. Gutiérrez, J. H. Kang, W. C. Chung, R. M. Fernandes, S. Jia, A. J. Millis, R. J. Cava, and A. N. Pasupathy, Visualizing the charge density wave transition in 2H-$NbSe_2$ in real space, Phys. Rev. B **89**, 235115 (2014).

[40] E. Oh, G. Gye, and H. W. Yeom, Defect-selective charge-density-wave condensation in 2H-$NbSe_2$, Phys. Rev. Lett. **125**, 036804 (2020).

[41] U. P. Sahoo, A. Mukherjee, and P. K. Sahoo, Short-Range charge density wave and bandgap modulation by Au-Implanted defects in $TiSe_2$, ACS Appl. Electron. Mater. **4**, 3428 (2022).

[42] C. Brun, Z.-Z. Wang, P. Monceau, and S. Brazovskii, Surface charge density wave phase transition in NbS_3, Phys. Rev. Lett. **104**, 256403 (2010).

[43] E. Machado-Charry, P. Ordejón, E. Canadell, C. Brun, and Z. Z. Wang, Analysis of scanning tunneling microscopy images of the charge-density-wave phase in quasi-one-dimensional $Rb_{0.3}MoO_3$, Phys. Rev. B **74**, 155123 (2006).

[44] C. Brun, E. Machado-Charry, P. Ordejón, E. Canadell, and Z. Z. Wang, Inhomogeneities of the CDW vector at the (-201) surface of Quasi-1D blue bronze $Rb_{0.3}MoO_3$, J. Phys.: Conf. Ser. **61**, 140 (2007).